Master curve of boosted diffusion for 10 catalytic enzymes

Ah-Young Jee[a], Tsvi Tlusty[a,b], and Steve Granick[a,b,c,1]

[a]Center for Soft and Living Matter, Institute for Basic Science, Ulsan 44919, Republic of Korea; [b]Department of Physics, Ulsan National Institute of Science and Technology, Ulsan 44919, Republic of Korea; and [c]Department of Chemistry, Ulsan National Institute of Science and Technology, Ulsan 44919, Republic of Korea

Contributed by Steve Granick, October 2, 2020 (sent for review September 21, 2020; reviewed by Mischa Bonn and Steve Pressé)

Molecular agitation more rapid than thermal Brownian motion is reported for cellular environments, motor proteins, synthetic molecular motors, enzymes, and common chemical reactions, yet that chemical activity coupled to molecular motion contrasts with generations of accumulated knowledge about diffusion at equilibrium. To test the limits of this idea, a critical testbed is the mobility of catalytically active enzymes. Sentiment is divided about the reality of enhanced enzyme diffusion, with evidence for and against. Here a master curve shows that the enzyme diffusion coefficient increases in proportion to the energy release rate—the product of Michaelis-Menten reaction rate and Gibbs free energy change (ΔG)—with a highly satisfactory correlation coefficient of 0.97. For 10 catalytic enzymes (urease, acetylcholinesterase, seven enzymes from the glucose cascade cycle, and one other), our measurements span from a roughly 40% enhanced diffusion coefficient at a high turnover rate and negative ΔG to no enhancement at a slow turnover rate and positive ΔG. Moreover, two independent measures of mobility show consistency, provided that one avoids undesirable fluorescence photophysics. The master curve presented here quantifies the limits of both ideas, that enzymes display enhanced diffusion and that they do not within instrumental resolution, and has possible implications for understanding enzyme mobility in cellular environments. The striking linear dependence of ΔG for the exergonic enzymes ($\Delta G < 0$), together with the vanishing effect for endergonic enzyme ($\Delta G > 0$), are consistent with a physical picture in which the mechanism boosting the diffusion is an active one, utilizing the available work from the chemical reaction.

enzyme | diffusion | enhanced | catalysis | FCS

We are interested in the diffusive-looking random walks executed when chemical reactions inject energy into the system, kicking it off equilibrium. Bacteria and active colloids, for example, are propelled along trajectories that appear diffusive at long timescales but are more persistent and superdiffusive at shorter timescales (1). Recent reports of "enhanced" or "boosted" diffusion of various molecules extend this notion down to the molecular scale, raising questions about the shared and distinguishing features of equilibrium and nonequilibrium, not only for protein molecular motors where the phenomenon was first identified (2), but also for synthetic molecular motors (3–5), active fluctuations in the cell (6, 7), optically trapped colloids (8), common chemical reactions (9), and enzymes (10–18). Regarding enzymes, however, experiments have not tackled the basic question of how the reaction rate and the free energy released affect mobility. Moreover, measuring boosted enzymatic motion has proven challenging, as it is a rapid process occurring over length scales of a few nanometers. Some studies assert that the apparent enhancement originates from experimental artifacts (19–22), as has been reviewed critically (23).

In the present work, we investigated 10 different enzymes whose energy release rate varies over a wide range, using two independent instrumental methods. Tracing the enzymatic reaction rate, we find a strikingly simple dependence of diffusivity on rate, thus quantifying the coupling of mobility and chemical activity.

Results

Experimental Design. Our experimental design is guided by the following considerations. To minimize chemical differences, for two of the enzymes we tuned the catalytic activity by varying temperature and pH independently. To test the validity of fluorescence measurements, we compared them with independent measurements with a complementary technique, dynamic light scattering (although only fluorescence can probe the most desirably dilute concentrations). We selected enzymatic reactions whose Gibbs free energy change, ΔG, and the turnover rate, k_{cat}, are either known from the literature or can be measured by us. Urease was included in several early studies reporting enhanced diffusion (11, 13–18) and thus was included here, while keeping in mind that the hydrolysis of urea releases CO_2. This effect is potentially confounding, as whether CO_2 is fully dissolved or forms bubbles is unclear, but the consistency that we report with the other enzymes suggests the former. We excluded catalase (12–14), because its reaction produces visible oxygen bubbles that can generate the appearance of convection-induced enhanced diffusion for spurious reasons (24). To avoid the reported tendency of multimeric enzymes to dissociate when the substrate concentration exceeds a level roughly equal to the Michaelis constant (18), we were careful not to exceed this limit. We avoided aggregation caused by high enzyme concentration (18). Finally, a major design consideration was selecting enzymes whose catalytic turnover rates vary widely, from relatively fast for some enzymes to relatively slow for others. On physical grounds,

Significance

The literature is inconsistent regarding evidence for boosted molecular mobility during enzyme catalysis, a phenomenon that challenges the common tenet that enzyme mobility is governed solely by Brownian motion. This paper surveys 10 different catalytic enzymes and shows that magnitude of enhanced diffusion scales with energy release rate, the Gibbs free energy of reaction multiplied by the Michaelis–Menten reaction rate. A practical implication is that boosted effective diffusivity can be used to determine the energetics associated with enzyme action, since effective enzyme diffusivity is simply proportional to the change in free energy associated with the biochemical conversion. This master curve to predict the magnitude of boosted molecular mobility may be useful for estimating the effect in as-yet untested enzymes.

Author contributions: A.-Y.J. and S.G. designed research; A.-Y.J. performed research; A.-Y.J., T.T., and S.G. analyzed data; and A.-Y.J. and S.G. wrote the paper.

Reviewers: M.B., Max Planck Institute for Polymer Research; and S.P., Arizona State University.

The authors declare no competing interest.

See online for related content such as Commentaries.

[1]To whom correspondence may be addressed. Email: sgranick@gmail.com.

First published November 9, 2020.

we hypothesized that if catalysis events induce enhanced diffusion, then the effect should increase with turnover rate.

The 10 enzymes that we studied are summarized in Table 1. For each enzyme, the table lists its turnover rate, k_{cat}; Michaelis constant, k_M; free energy of reaction, ΔG_{rxn}; diffusion coefficient, D_0, measured in this laboratory in the absence of substrate; and maximal boosted diffusion at 25 °C. Among the seven exergonic enzymes ($\Delta G < 0$), urease was selected, because it is the enzyme for which enhanced diffusion was first reported (11); here we extended the range of k_{cat} values by varying temperature and pH. For acetylcholinesterase (AChE), we also extended the range of k_{cat} beyond that used in the original study (15, 16) by varying temperature and pH. The other enzymes—aldolase, phosphoglucoisomerase, pyruvate kinase, hexokinase, and phosphofructokinase—were selected from the glucose cascade cycle (25). Among the three endergonic reactions ($\Delta G > 0$), alkaline phosphatase and triosephosphate isomerase were selected, to repeat the measurements of an earlier study (14, 21), and phosphoglycerate kinase was selected from the glucose cascade cycle. The substrate concentrations were selected to give reaction half-lives of a few minutes.

Each of our data points represents the average of 20 to 30 repeated independent measurements. For many measurements, we used fluorescence correlation spectroscopy (FCS), a standard method of measuring molecular diffusion in the nanomolar range (*Methods*). The principle of FCS measurement is that fluorescence intensity fluctuates due to molecules diffusing into and out of tiny spaces whose volumes are diffraction-limited. We also used dynamic light scattering (DLS), another standard method that quantifies the photon autocorrelation function and extracts from it the implied translational diffusion coefficient. FCS has the advantage of greater sensitivity. DLS is less sensitive but has the advantage of no need for labeling. While pushing the limits of DLS sensitivity, in some cases we were able to almost match the enzyme concentration in both experiments.

Boosted Diffusion Correlates with Reaction Rate. Boosted diffusion during enzyme-catalyzed chemical reactions was normalized to Brownian diffusion as $\Delta D/D_0$, where $\Delta D = D - D_0$, D is the enzyme diffusion coefficient during chemical reaction, and D_0 is the bare thermal diffusion coefficient in the absence of substrate or when the reaction is complete. Standard Michaelis–Menten reaction kinetics give the substrate concentration, $c(t)$, and reaction rate, $V(t) = k_{cat}\, c(t)/(K_M + c(t))$. For three representative reactions plotted against time, catalyzed by the enzymes phosphoglucoisomerase, AChE, and urease, the reaction rate, $V(t)$, and the enhanced diffusion, $\Delta D(t)/D_0$, decay over the same time scale (Fig. 1*A*) with the same fractional changes; their ratio is unity within the experimental uncertainty (Fig. 1*B*). Therefore, $\Delta D/D_0\ (t)$ is directly proportional to $V(t)$. Fluorescence-based measurements agree quantitatively with an independent DLS measurement (Fig. 1*B*).

Experimental Validation of FCS. Before presenting our main results, we examine the scope and limitations of this treatment and its relationship to previous empirical and theoretical discussions of the enhanced enzyme diffusion problem. To check the reliability of our FCS data, we performed direct tests of fluorophore photostability. To find a fluorophore whose photostability allows the deduction of diffusion from the FCS intensity-intensity autocorrelation curve, we screened candidate dyes and selected Atto 488 based on the observation that its fluorescence lifetime decay, when bound to the enzymes of interest, was the same in the presence or absence of substrate under the respective buffer conditions of each enzyme reaction. Likewise, in three cases studied explicitly, we confirmed that fluorescence lifetime decay, when bound to enzymes of interest, was unaffected by the presence of product without substrate.

To illustrate this phenomenon, fluorescence intensity decay on the nanosecond timescale, measured using time-correlated single photon counting, is plotted for pyruvate kinase, hexokinase, and AChE (enzymes 3, 4, and 6, respectively) in Fig. 1*C*. All fluorescence decay curves were nonexponential, as is typically found given the multiple mechanisms of excited state deactivation (26). We fitted them by double-exponential functions. Because both timescales affected the overall fluorescence lifetime, the average fluorescence lifetime $\langle\tau\rangle$ (with $\langle\tau\rangle = A_1\tau_1 + A_2\tau_2$, $A_1 + A_2 = 1$) was used for further analysis. For all 10 enzymes, Fig. 1*D* shows the average fluorescence lifetime at room temperature for Atto 488 in the presence or absence of substrate. For three of the enzymes, the figure includes data for product present without substrate. In contrast, some of the enzymes labeled with the commonly used dyes Alexa Fluor 488 and Cy3 (Fig. 1*E*) showed a significant decrease in lifetime during the respective chemical reactions that they catalyzed. Thus, although these latter two dyes are sometimes considered a gold standard, we did not use them in our subsequent measurements. These precautions were necessary to avoid the known corrupting influence that photophysical changes, such as photobleaching and reversible quenching, can have on fluorescence intensity-intensity fluctuations, shifting the autocorrelation curve to shorter times for this spurious reason (22, 27).

Table 1. Enzyme specifications

Code	Enzyme	k_{cat} (s^{-1})	K_M (mM)	ΔG (kJ/mol)	D_0 ($\mu m^2/s$)	$\Delta D/D_0$ (25 °C)
1	Fructose bisphosphate aldolase	5–42 (18–20, 47)	0.12	−1.3(48)	55 ± 2.4	0.01
2	Phosphofructokinase	150 (49)	0.15 (49)	−26 (50)	53 ± 3.2	0.03
3	Pyruvate kinase	232 (51)	0.1 (51)	−33.4 (50)	65 ± 3.3	0.037
4	Hexokinase	250 (18)	0.04	−33.5 (48)	64 ± 2.6	0.04
5	Phosphoglucoisomerase	3330 (52)	1.5	−2.92 (31)	62 ± 2.4	0.1
6	Acetylcholinesterase	14,000 (18) measured here;	0.5 (18)	−17.6 (28)	45 ± 1.8	0.18
7	Urease	17,000 measured here; 2,000~45,000 (11, 18, 53)	3	−21.5 (54)	39 ± 1.2	0.24
8	Phosphoglycerate kinase	685 (55)	0.27	+1.3 (55); +90 (56) +20.9 (57)	65 ± 3.1	0
9	Triosephosphate isomerase	13,000 (14)	1.8 (14)	+2.5 (48); +47.3 (58)	61 ± 2.8	0
10	Alkaline phosphatase	14,000 (14); 95 (29)	1.3 0.0003	+30.2 (28); +61.5 (29)	54 ± 2.0	0

The table lists code numbers to identify each enzyme and its turnover number, k_{cat}; Michaelis–Menten constant, K_M; Gibbs free energy of reaction, ΔG; diffusion coefficient measured in the absence of substrate, D_0; and relative enhanced diffusion, $\Delta D/D_0$, measured at the earliest measurement times.

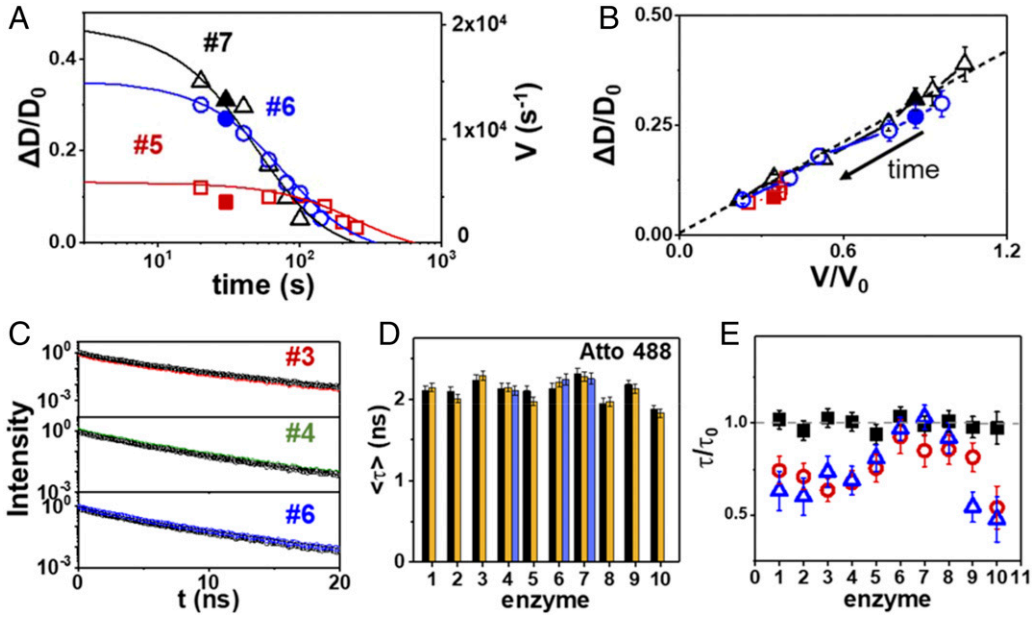

Fig. 1. (*A* and *B*) Boosted enzyme diffusion $\Delta D/D_0$ scales with reaction rate. (*A*) $\Delta D/D_0$ (left ordinate) and reaction rate V (right ordinate) plotted against time (log scale) for enzymes 5 (squares), 6 (circles), and 7 (triangles) from Table 1, measured by FCS (empty symbols) and DLS (filled symbols) at 25 °C. Solid lines are calculated from k_{cat} using first-order reaction kinetics. (*B*) Same data replotted as $\Delta D/D_0$ as a function of V/V_0 with the same symbols. The dashed line shows the linear relation. (*C*–*E*) Fluorescence lifetime decay, using Atto 488 dye, is constant across all 10 enzyme systems under the respective buffer conditions of each enzyme reaction. (*C*) Raw data illustrating fluorescence lifetime decay of enzymes 3, 4, and 6 in the presence (colored symbols) and absence (black symbols) of substrate. (*D*) Bar graphs comparing the average fluorescence lifetime $\langle\tau\rangle$ for all 10 enzymes in the presence (yellow bars) and absence of substrate for Atto 488 dye and for three enzymes in the presence of product but not substrate (blue bars). (*E*) Ratio of average fluorescence lifetime $\langle\tau\rangle$ with and without substrate for all 10 enzymes for Atto 488 (black squares), Alexa Fluor 488 (red circles), and Cy3 (blue triangles).

Inconsistent findings in the enzyme community can be attributed in part to the use of different fluorescent probes. In what follows, we report the consistency of FCS and DLS measurements for various temperature and pH conditions.

Master Curve of Boosted Diffusion for 10 Enzymes. The seven exergonic (ΔG <0) enzymes listed in Table 1 exhibit boosted diffusion with a magnitude proportional to the reaction rate V with a correlation coefficient of 0.650 (Fig. 2*A*). Multiplying V by $-\Delta G$ yields the energy release rate. We see that the boosted diffusion, $\Delta D/D_0$, is directly proportional to the energy release rate, with a correlation coefficient of 0.986 for measurements at 25 °C (Fig. 2*B*) and 0.970 when measurements at all temperatures and pH are included (Fig. 2*C*). In contrast, these data do not significantly correlate with the enthalpy change, ΔH (Fig. 3*A*), nor with the enthalpy release rate, $V(-\Delta H)$ (Fig. 3*B*).

One notable case is the enzyme alkaline phosphate, which catalyzes a highly exothermic reaction with $\Delta H = -43.5$ kJmol^{-1} yet positive $\Delta G = +30.2$ (28) or +61.5 (29) kJmol^{-1} at a high turnover rate. This shows no detected enhanced diffusion, in agreement with a recent earlier study (21). Therefore, we consider it more meaningful physically to seek a correlation with ΔG, the maximum available work that can be extracted from the reaction (15, 16). Moreover, heat release would dissipate too rapidly to induce enhanced diffusion (16, 30). At these ultralow enzyme concentrations (nanomolar), we found no dependence on enzyme concentration; the master curve in Fig. 2 *B* and *C* appears to be a single-enzyme property, not a collective effect. The striking linear dependence of ΔG for the exergonic enzymes (ΔG <0), together with the vanishing effect for endergonic enzyme (ΔG >0), are consistent with a physical picture in which the mechanism boosting the diffusion is an active one, using the available work from the chemical reaction.

Temperature and pH Dependence of Boosted Diffusion. Our dataset includes experiments in which we tuned temperature and pH to compare the same enzyme at different k_{cat} values. Because enzyme functional groups at and near active sites have a wide range of pK_a values (the index to express the acidity), changes in temperature and pH alter their charge makeup and thus modulate their catalytic efficiency and turnover rate. Standard enzyme assays were performed to measure enzyme activity under each of these conditions. The k_{cat} values for urease and AChE were inferred from standard Lineweaver–Burk plots with excellent fits of Michaelis–Menten parameters (Fig. 4 *A* and *B*). For both enzymes, the turnover rate increased monotonically with temperature (Fig. 4*C*). With pH varied at room temperature (Fig. 4*D*), it showed a maximum at pH 7.

The limits of temperature and pH that we studied were set by enzyme stability. It is reassuring that the Gibbs free energy (ΔG) values implied by the temperature data, −21.05 and −16.16 kJ/mol for urease and AChE, respectively, are consistent with known values (28, 31). To orient the reader, a typical small protein with diffusion coefficient, D, of ∼50 μm^2-s^{-1} and a k_{cat} of ∼10^3 s^{-1} diffuses at equilibrium the root mean square distance of ∼100 nm in 1 ms, the average time between its catalytic events.

Comparison of FCS and DLS at Various Temperature and pH. DLS validated the consistency of fluorescence-based FCS measurements. Our DLS tests were performed on enzymes labeled in the same manner as for the FCS experiments, with the same buffer conditions and at the same temperature (*Methods*). Working within the constraint that DLS is less sensitive than FCS and thus demands higher enzyme concentrations, we used DLS enzyme concentrations as close as possible to those used for FCS. Fig. 4 *E* and *F* shows quantitative agreement in measurements of urease (7) and AChE (6), both in measurements obtained at pH 7 and different temperatures (Fig. 4*E*) and in measurements

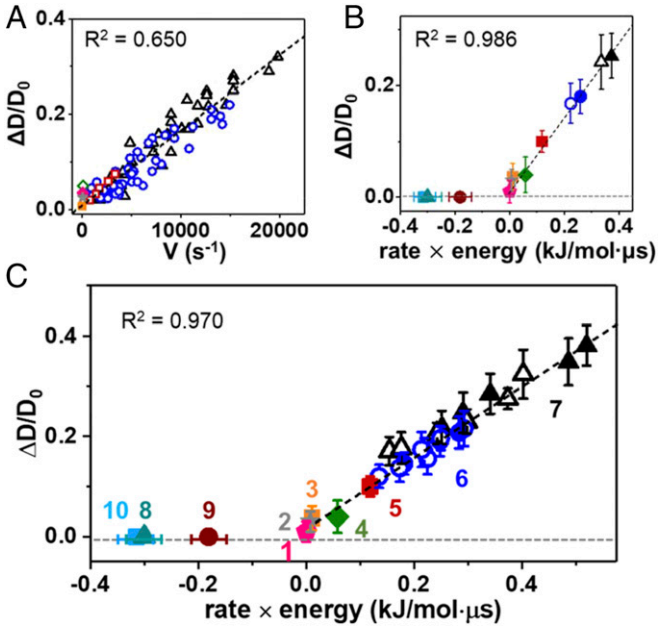

Fig. 2. Master curves. (*A*) $\Delta D/D_0$ plotted against the reaction rate V for the seven exergonic enzymes (ΔG <0, 1 to 7 in Table 1); symbols are as in *C*. (*B*) For measurements at 25 °C, $\Delta D/D_0$ plotted against the product of V and ($-\Delta G$), the free energy release rate. For the three endergonic enzymes (ΔG >0), $\Delta D/D_0 = 0$. Symbols are as in *C*. (*C*) $\Delta D/D_0$ plotted against V ($-\Delta G$), the free energy release rate. Horizontal error bars for enzyme phosphoglycerate kinase (8), triosephosphate isomerase (9), and alkaline phosphate (10) reflect the range of reported k_{cat} values (Table 1). Symbols are identified by enzyme code in Table 1. Data were obtained at 25 °C and constant pH except for auxiliary measurements with temperature and pH varied for enzymes 6 and 7; details given in Fig. 4. The units of energy release, here in kJ/mol·μs, are equivalent to k_BT/μs per molecule (k_BT = 2.479 kJ/mol).

obtained at 25 °C and different pH values (Fig. 4*F*). Diffusion coefficients measured by these independent methods agree within the experimental uncertainty.

Discussion

We use the term "boosted diffusion" to emphasize that this phenomenon is associated with chemical activity such that released chemical energy generates persistent motion (9, 15, 16) and thereby increases mobility. In this view, endergonic reactions (ΔG >0) are predicted to show no boosted mobility, as was observed, while the boosts in the exergonic enzymes (ΔG <0) collapse on one master curve because they have similar timescales of reorientation and boost from the chemical reaction (16). While enhanced diffusion is observable only for high-turnover enzymes, in principle it may also occur in slower enzymes, where it is masked by dominant Brownian motion.

The master curve that we have presented is broadly consistent with that from a parallel study of nonenzymatic chemical reactions (9, 16), but that study showed considerably more scatter, probably because those reactions have more complex intermediate states in a variety of solvents, whereas the present reactions lack complex intermediates, and the solvent is always aqueous solution. Theoretically, different underlying mechanisms have been proposed, including conformational changes (30, 32, 33) cross-diffusion (34, 35), exothermicity (14), momentum exchange (36), and solvation shifts owing to electronic rearrangements during chemical reactions (9). In short, the theoretical community is aware of the enhanced diffusion problem and is actively working to come up with an underlying physical mechanism—a difficult task, since one needs to link normal liquid dynamics to the quantum chemistry at the Angstrom regime of enzymatic reactions. This theoretical challenge lies within the realm of "active matter" research (1) and the idea that the conversion of chemical energy to kinetic energy by impulsive enzymes is a force in mechanobiology (37). The empirical correlations presented here are quite independent of their theoretical specific mechanistic origin and may serve as a phenomenologic guide for further investigation.

The mobility that we study here differs from the "micromotor" situation in which catalytically active enzymes (urease in many instances) are attached chemically to colloids or vesicles and their enhanced mobility is observed after the addition of substrate (38–42). Micromotors are driven by a concentration gradient of reaction products near the surfaces of colloidal beads, a phenomenon known as diffusiophoresis (43–45). Diffusiophoresis is not believed to contribute to the situations considered here, unlike the case of the concentration gradients that underpin the diffusiophoresis of colloids and vesicles. Simply put, the nanometer size of enzymes and their nanomolar concentrations are too small to allow the establishment of concentration gradients across these molecules.

Physically, the magnitudes of $\Delta D/D_0$ and their proportionality to the reaction rate that we observe suggest that the energy released by chemical reactions transiently propels enzymes at the nanoscale during catalytic events. Accompanied by random thermal reorientation and translation, these boosts produce random yet persistent motion over distances vastly exceeding the molecular dimensions. In previous work, we analyzed this phenomenon for two specific enzymes (15, 16). The precise magnitude of diffusion enhancement that can be extracted from a given amount of free energy released turns out to be sensitive to parameters not yet known from direct experiments (16, 23).

Quantitatively elucidating the nature of boosts stimulated by chemical reactions is a research challenge, but a basic assumption of this proposed scenario is that a significant part of the released free energy,$-\Delta G$, is transduced into persistent motion of the enzyme along distances of a few nanometers and durations of a few microseconds. We previously presented a simple theoretical model for this process (16). As the enzyme is thrust along this stochastic wormlike trajectory, viscous forces gradually dissipate the released free energy into smaller and faster thermalized degrees of freedom of solvent molecules. We recognize that the proposed physical scenario is speculative at this stage of theoretical understanding. It is quite different from the standard textbook view of chemical reactions in which energy released by a chemical reaction is transduced into thermal motion of the solvent directly as heat.

This common mode of enhanced diffusion in living systems (46) thus generalizes pleasingly to enzyme macromolecules when they likewise consume energy by catalyzing chemical reactions. The master curve that we have introduced based on experimental data may have functional implications for how reaction

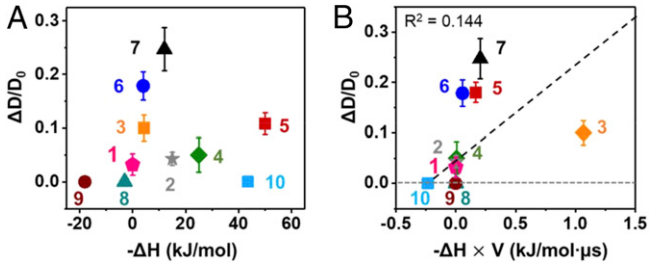

Fig. 3. Boosted diffusion showing minimal correlation with enthalpy of reaction. (*A*) $\Delta D/D_0$ plotted against ΔH. (*B*) $\Delta D/D_0$ plotted against the enthalpy release rate, $V(-\Delta H)$. The dotted line, the best linear fit, has $R^2 = 0.15$, significantly weaker than the $R^2 = 0.970$ shown in Fig. 2*D*.

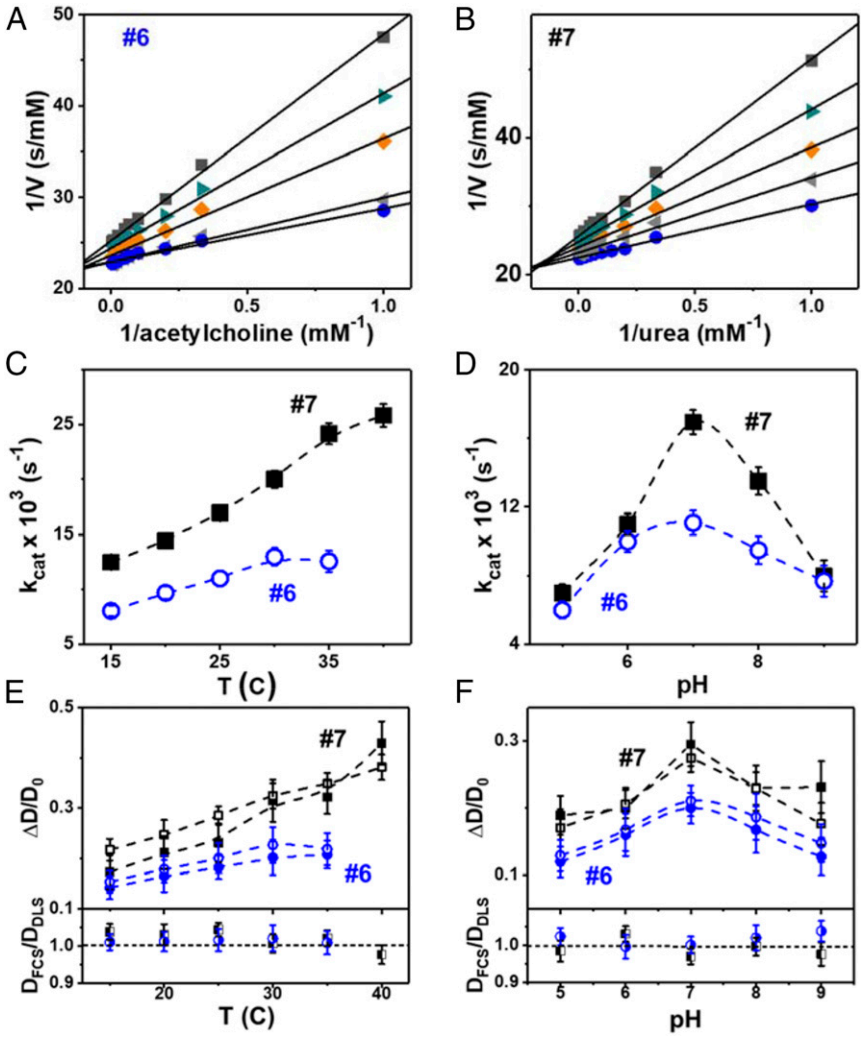

Fig. 4. Adjusting k_{cat} according to temperature and pH with diffusion measured using independent methods. (*A* and *B*) Lineweaver–Burk plots for AChE (*A*) and urease (*B*) to deduce k_{cat}. The inverse reaction rate is plotted against the inverse substrate concentration. (*C* and *D*) The deduced k_{cat} plotted against temperature (*C*) and pH (*D*) for AChE (circles) and urease (squares). (*E* and *F*) Dynamic light scattering validates FCS measurements. (*E*) $\Delta D/D_0$ measured by DLS (filled symbols) and FCS (open symbols) plotted against temperature for the enzymes AChE (6; blue circles) and urease (7; black squares). (*Lower*) The ratio of D_{FCS}/D_{DLS} at each temperature. (*F*) $\Delta D/D_0$ plotted against pH for enzymes 6 (blue circles) and 7 (black squares). (*Lower*) D_{FCS}/D_{DLS} at each pH value.

rate and substrate availability regulate enzyme diffusion in cellular environments where unambiguous measurement of single-enzyme diffusion is presently not feasible. A practical implication is that this boosted effective diffusivity can be used to determine the energetics associated with enzyme action, since the effective enzyme diffusivity is simply proportional to the change in free energy associated with the biochemical conversion.

Methods

Enzyme Samples and Dye Labeling. Urease (type C-3) from jack bean, purchased from Sigma-Aldrich, was labeled at the cysteine residue with Dylight 488 maleimide dye by a protocol involving 150 mM phosphate buffer (pH 7.2) with added 2 μM urease and 40 μM fluorescent dye solution, stirred for 6 h at room temperature. Acetylcholinesterase from *Electrophorus electricus* (electric eel), purchased from Sigma-Aldrich, was labeled at its amine residue by Dylight 488-NHS (*N*-hydroxysuccinimide) dye using a protocol in which 30 μM dye solution and 1 μM enzyme were added to a mixture of 80% PBS and 20% DMSO, followed by 6 h of stirring at room temperature. Finally, the dye-labeled enzymes were purified by removing the free dye by membrane dialysis (Amicon Ultra-4 centrifugal filter; Millipore Sigma). Hexokinase I from *Saccharomyces cerevisiae* was purchased from Sigma-Aldrich and labeled with an Alexa Fluor 488 labeling kit (Invitrogen) using a protein fluorescence labeling kit (Invitrogen). Fructose bisphosphate aldolase from rabbit muscle, pyruvate kinase (type III), phosphoglucose isomerase (type III) from baker's yeast, fructose-6-phosphate kinase (type VII) from *Bacillus stearothermophilus*, 3-phosphoglyceric phosphokinase from baker's yeast, triosephosphate isomerase from rabbit muscle, and alkaline phosphatase from *Escherichia coli* were purchased from Sigma-Aldrich and labeled with an Alexa Fluor 488 labeling kit (Invitrogen), an Atto 488 protein labeling kit (Sigma-Aldrich), and a Cy3 protein labeling kit (Sigma-Aldrich). For the enzymes that we also studied previously, these methods follow our earlier protocol (15, 16, 18).

For fluorescence labeling, a new, freshly opened bottle of enzyme was used each time. Newly labeled enzymes were used within 2 to 3 d at the longest. Enzyme solutions were stored at 4 °C.

During dye labeling, reaction times were selected to give at most one dye per enzyme on average as determined from comparing UV-Vis absorbance measurements of the enzyme and dye-labeled enzyme. Consistent D_0 measured using DLS with and without dye-labeling showed that labeling with a single dye molecule (<1 nm) produced no detectable change in D_0.

Enzyme Substrates. Fructose-1,6-bisphosphate (aldolase reaction), fructose-6-phosphate (phosphofrucokinase reaction), phosphoenolpyruvate (pyruvate kinase reaction), glucose (hexokinase reaction), glucose-6-phosphate (phosphoglucose isomerase reaction), acetylcholine (AChE reaction), urea (urease reaction),

p-nitrophenylphosphate (alkaline phosphatase reaction), glycerol 3-phosphate dehydrogenase (triosephosphate isomerase reaction), 3-phosphoglycerate (phosphoglucerate kinase reaction).

Experimental Procedure. Bearing in mind that vortex mixing can denaturate proteins, the solutions were mixed by gentle pipetting. In our reported values of $\Delta D/D_0$ as a function of temperature and pH, D_0 was measured separately without substrate at each of these conditions. Measurements by FCS began 30 s after mixing. FCS measurements lasting 30 s were repeated 20 to 30 times. First, an enzyme preparation was divided into 10 aliquots, and each aliquot was measured independently in repeat experiments, each time with fresh substrate. The next day, a new enzyme preparation was prepared, and this procedure was repeated. In some cases, the procedure was repeated on the third day. DLS measurements were made immediately after 5 s of mixing. For DLS, 30 nM Atto 488-labeled enzyme was added to 50 mM substrate, and measurements were made for 50 s, which is the initial half-reaction time. The enzyme concentration used for DLS was selected to be the lowest at which photon autocorrelation curves of sufficient quality were achieved. Error bars show the SD.

Enzyme Activity Assays. The urease and AChE were performed using a urease activity kit (MAK120; Sigma-Aldrich) and an AChE activity kit (MAK119; Sigma Aldrich) following the manufacturer's instructions. The activities of other enzymes listed in Table 1 were obtained from the references cited in the table.

FCS. In preparation for FCS measurements, dye-labeled enzyme was mixed with substrate in the appropriate aqueous buffer. To study urea (Sigma-Aldrich), 2 nM dye-labeled urease was added at room temperature (100 mM PBS buffer, pH 7.2). When studying AChE, 2 nM dye-labeled AChE was added in acetylthiocholine (Sigma-Aldrich) at room temperature (100 mM PBS buffer, pH 7). For studying hexokinase, 2 nM of dye-labeled hexokinase I was added to a medium containing 50 mM Tris·HCl pH 7.5, 0.5 mM $MgCl_2$, 0.12 mM ATP, 0.1 mM $NAD(P)^+$, and 0.03 mM glucose. For studying aldolase, 2 nM of dye-labeled aldolase was added to 50 mM Hepes buffer (pH 7.4) and mixed with 0.1 mM of fructose-1,6-bisphosphate. The pyruvate kinase reaction was carried out by adding 2 nM pyruvate kinase in a reaction buffer containing 50 mM potassium phosphate pH 7.0, 30 mM potassium chloride, 1 mM $MgCl_2$, 0.1 mM ADP, 0.1 mM P-enolpyruvate, 1 mM ATP, and 0.1 mM pyruvate. For studying phosphoglucoisomerase, 2 nM of phosphoglucoisomerase was added to 1 mM glucose-6-phosphate dissolved in 20 mM Tris·HCl buffer pH 7.7. For studying phosphofructokinase, 1 nM phosphofructokinase was added to 0.1 mM fructose-6-phosphate, ATP 0.5 mM, NADH 0.2 mM, and 20 mM Tris-HC1 buffer pH 7.9. For the alkaline phosphatase reaction, enzyme was dispersed in diethanolamine 2 M pH 9.8, 1 mM $MgCl_2$, and 20 mM $ZnCl_2$, with 1 mM of p-nitrophenylphosphate (Sigma). The triosephosphate isomerase reaction was performed in triethanolamine 100 mM, pH 7.9, in the presence of 0.125 mM NADH and 1 mM glycerol 3-phosphate dehydrogenase (Sigma-Aldrich) with 2 nM enzyme. For phosphoglycerate kinase reaction, 2 nM dye-labeled phosphoglycerate kinase was dispersed in 20 mM Tris·HCl pH 7.5, 5 mM $MgCl_2$, 5 mM ATP, 0.2 mM NADH, and 0.2 mM 3-phosphoglycerate. For the enzymes studied previously, this methodology follows our earlier protocol (15, 16, 18).

All fluorescence measurements were made in the presence of a standard photobleaching agent: a stock agent made by dissolving trolox (2 mM), cyclooctatetraene (1 mM), and nitrobenzyl alcohol (1.5 mM) (Sigma-Aldrich) in 1 mL DMSO. This agent was added to each reaction to a final 1/10 dilution (59, 60).

FCS measurements were performed with an inverted microscope (Leica TCS SP8X), using a 100× oil immersion objective lens with numerical aperture of 1.4 and pinhole size equal to 1 airy unit as described previously (15, 16, 18). Emitted fluorescence was collected using an avalanche photodiode (APD; Micro Photon Devices; PicoQuant) through a 500- to 550-nm bandpass filter. The excitation power was controlled up to 20 μW. The APD signal was recorded using a time-correlated single photon-counting (TCSPC) detection unit (Picoharp 300; PicoQuant).

To begin, the samples—substrate solutions (hundreds of mM) and a relatively high (50 nM) concentration of dye-labeled enzyme—were equilibrated in a water bath at the desired temperature for approximately 10 min. Temperature during the FCS measurements was controlled at the sample stage and the objective lens. The enzyme solution was loaded into a Nunc 1 coverslip eight-chamber slide (Lab-Tek chambered coverglass; Thermo Fisher Scientific) and mixed with a small aliquot of substrate solution to give an enzyme concentration <2 nM with the desired sub-mM substrate concentration in a total volume of 300 μL. FCS measurement began approximately 30 s after mixing.

The FCS setup was freshly aligned for each channel on the day of use. This was done using a dye solution with a known diffusion coefficient (1 to 10 nM) and with similar excitation and emission wavelengths as the sample of interest; we selected solutions of Alexa Fluor 488 (D = 435 $\mu m^2/s$). The calibration chamber was equivalent to that used to measure samples. For calibration and subsequent experiments, first we measured scattering from the coverslip glass surface to determine its location, then focused 10 μm into the solution. Our control experiments showed that the diffusion coefficient of reference and enzyme sampled did not depend on focus position in the range of 5 to 12 μm.

Inspecting the autocorrelation curve, $G(t)$, of the reference solution with the standard 3D diffusion model, the focus waist and height were calibrated. The structure factor f, the ratio of height to width of the focus beam, varied from day to day in the range of 6∼8, and the $G(t)$ of samples was fitted using SymPhoTime software (PicoQuant). The day-to-day variability was less than the variability between measurements recorded the same day. Data acquisition times were 30 s. Enzyme reaction is not expected to change the confocal volume; thus, uncertainties in calibrating the confocal volume are not believed to influence the relative measurements on which this study focuses.

Fluorescence Lifetime Measurement. The lifetime experiments (Leica TCS SP8X) used a 100× oil immersion objective lens with numerical aperture 1.4, an excitation wavelength of 488 nm with excitation at 80 MHz, and a pulse width of 80 ps, following our earlier protocol (18). Emitted fluorescence was collected using an APD (Micro Photon Devices; PicoQuant) through a 500- to 550-nm bandpass filter and recorded using a TCSPC detection unit (Picoharp 300; PicoQuant) integrated into the microscope that saves detected photons on the fly as data are acquired. This allows for reconstruction of fluorescence lifetime decays using SymPhoTime.

DLS. A Brookhaven ZetaPALS instrument with the ZetaPlus option at a 90° scattering angle and a temperature control function was used at the IBS Center for Multidimensional Carbon Materials, following our earlier protocol (18). For DLS measurements, 30 nM dye-labeled enzymes (urease and AChE) and the substrate solution (urea for urease, acetylthiocholine for AChE) were mixed at the desired concentration in 100 mM PBS buffer (pH 7.2) and filtered twice using a 100-nm pore size syringe filter (Whatman).

Data Availability. All study data are included in the main text.

ACKNOWLEDGMENTS. This work was supported by the taxpayers of the Republic of Korea through the Institute for Basic Science (Project Code IBS-R020-D1).

1. C. Bechinger *et al*., Active particles in complex and crowded environments. *Rev. Mod. Phys.* **88**, 045006 (2016).
2. R. D. Vale, R. A. Milligan, The way things move: Looking under the hood of molecular motor proteins. *Science* **288**, 88–95 (2000).
3. A. Coskun, M. Banaszak, R. D. Astumian, J. F. Stoddart, B. A. Grzybowski, Great expectations: Can artificial molecular machines deliver on their promise? *Chem. Soc. Rev.* **41**, 19–30 (2012).
4. V. García-López *et al*., Molecular machines open cell membranes. *Nature* **548**, 567–572 (2017).
5. L. Pfeifer *et al*., Photoefficient 2nd generation molecular motors responsive to visible light. *Chem. Sci. (Camb.)* **10**, 8768–8773 (2019).
6. S. C. Weber, A. J. Spakowitz, J. A. Theriot, Nonthermal ATP-dependent fluctuations contribute to the in vivo motion of chromosomal loci. *Proc. Natl. Acad. Sci. U.S.A.* **109**, 7338–7343 (2012).
7. A. Agrawal, N. Ganai, S. Sengupta, G. I. Menon, Nonequilibrium biophysical processes influence the large-scale architecture of the cell nucleus. *Biophys. J.* **118**, 2229–2244 (2020).
8. J. T. Park, G. Paneru, C. Kwon, S. Granick, H. K. Pak, Rapid-prototyping a Brownian particle in an active bath. *Soft Matter* **16**, 8122–8127 (2020).
9. H. Wang *et al*., Boosted molecular mobility during common chemical reactions. *Science* **369**, 537–541 (2020).
10. H. H. Paradies, Effect of ATP on the translational diffusion coefficient of the α-subunit of Escherichia coli F1-ATPase. *FEBS Lett.* **120**, 289–292 (1980).
11. H. S. Muddana, S. Sengupta, T. E. Mallouk, A. Sen, P. J. Butler, Substrate catalysis enhances single-enzyme diffusion. *J. Am. Chem. Soc.* **132**, 2110–2111 (2010).
12. S. Sengupta *et al*., Enzyme molecules as nanomotors. *J. Am. Chem. Soc.* **135**, 1406–1414 (2013).
13. K. K. Dey *et al*., Micromotors powered by enzyme catalysis. *Nano Lett.* **15**, 8311–8315 (2015).
14. C. Riedel *et al*., The heat released during catalytic turnover enhances the diffusion of an enzyme. *Nature* **517**, 227–230 (2015).
15. A.-Y. Jee, S. Dutta, Y.-K. Cho, T. Tlusty, S. Granick, Enzyme leaps fuel antichemotaxis. *Proc. Natl. Acad. Sci. U.S.A.* **115**, 14–18 (2018).

16. A.-Y. Jee, Y.-K. Cho, S. Granick, T. Tlusty, Catalytic enzymes are active matter. *Proc. Natl. Acad. Sci. U.S.A.* **115**, E10812–E10821 (2018).
17. M. Xu, J. L. Ross, L. Valdez, A. Sen, Direct single molecule imaging of enhanced enzyme diffusion. *Phys. Rev. Lett.* **123**, 128101 (2019).
18. A.-Y. Jee, K. Chen, T. Tlusty, J. Zhao, S. Granick, Enhanced diffusion and oligomeric enzyme dissociation. *J. Am. Chem. Soc.* **141**, 20062–20068 (2019).
19. Y. Zhang, M. J. Armstrong, N. M. Bassir Kazeruni, H. Hess, Aldolase does not show enhanced diffusion in dynamic light scattering experiments. *Nano Lett.* **18**, 8025–8029 (2018).
20. J.-P. Günther, G. Majer, P. Fischer, Absolute diffusion measurements of active enzyme solutions by NMR. *J. Chem. Phys.* **150**, 124201 (2019).
21. Z. Chen *et al*., Single-molecule diffusometry reveals no catalysis-induced diffusion enhancement of alkaline phosphatase as proposed by FCS experiments. *Proc. Natl. Acad. Sci. U.S.A.* **117**, 21328–21335 (2020).
22. J.-P. Günther, M. Börsch, P. Fischer, Diffusion measurements of swimming enzymes with fluorescence correlation spectroscopy. *Acc. Chem. Res.* **51**, 1911–1920 (2018).
23. M. Feng, M. K. Gilson, Enhanced diffusion and chemotaxis of enzymes. *Annu. Rev. Biophys.* **49**, 87–105 (2020).
24. T. S. MacDonald, W. S. Price, R. D. Astumian, J. E. Beves, Enhanced diffusion of molecular catalysts is due to convection. *Angew. Chem.* **58**, 18864–18867 (2019).
25. L. Stryer, J. M. Berg, J. L. Tymoczko, *Biochemistry* (WH Freeman & Co Ltd, ed. 5, 2002).
26. J. R. Lakowicz, *Principles of Fluorescence Spectroscopy* (Springer Science & Business Media, 2013).
27. H. N. Kandula, A.-Y. Jee, S. Granick, Robustness of FCS (fluorescence correlation spectroscopy) with Quenchers present. *J. Phys. Chem. A* **123**, 10184–10189 (2019).
28. R. Caspi *et al*., The MetaCyc database of metabolic pathways and enzymes and the BioCyc collection of pathway/genome databases. *Nucleic Acids Res.* **44**, D471–D480 (2016).
29. A. Homaei, Purification and biochemical properties of highly efficient alkaline phosphatase from Fenneropenaeus merguiensis brain. *J. Mol. Catal. B Enzym.* **118**, 16–22 (2015).
30. R. Golestanian, Enhanced diffusion of enzymes that catalyze exothermic reactions. *Phys. Rev. Lett.* **115**, 108102 (2015).
31. D. Voet, J. G. Voet, C. W. Pratt, *Fundamentals of Biochemistry: Life at the Molecular Level* (Wiley, Hoboken, NJ, 2013).
32. B. Hille, Ionic channels in excitable membranes: Current problems and biophysical approaches. *Biophys. J.* **22**, 283–294 (1978).
33. A. Onufriev, D. Bashford, D. A. Case, Exploring protein native states and large-scale conformational changes with a modified generalized born model. *Proteins* **55**, 383–394 (2004).
34. X. Zhao *et al*., Substrate-driven chemotactic assembly in an enzyme cascade. *Nat. Chem.* **10**, 311–317 (2018).
35. J. Agudo-Canalejo, P. Illien, R. Golestanian, Phoresis and enhanced diffusion compete in enzyme chemotaxis. *Nano Lett.* **18**, 2711–2717 (2018).
36. S. Eloul, W. C. K. Poon, O. Farago, D. Frenkel, Reactive momentum transfer contributes to the self-propulsion of Janus particles. *Phys. Rev. Lett.* **124**, 188001 (2020).
37. P. J. Butler, K. K. Dey, A. Sen, Impulsive enzymes: A new force in mechanobiology. *Cell. Mol. Bioeng.* **8**, 106–118 (2015).
38. X. Ma *et al*., Enzyme-powered hollow mesoporous Janus nanomotors. *Nano Lett.* **15**, 7043–7050 (2015).
39. A. C. Hortelão, T. Patiño, A. Perez-Jiménez, À. Blanco, S. Sánchez, Enzyme-powered nanobots enhance anticancer drug delivery. *Adv. Funct. Mater.* **28**, 1705086 (2018).
40. T. Patino *et al*., Self-sensing enzyme-powered micromotors equipped with pH-responsive DNA nanoswitches. *Nano Lett.* **19**, 3440–3447 (2019).
41. X. Arqué *et al*., Intrinsic enzymatic properties modulate the self-propulsion of micromotors. *Nat. Commun.* **10**, 2826 (2019).
42. X. Ma, A. C. Hortelao, A. Miguel-López, S. Sánchez, Bubble-free propulsion of ultrasmall tubular nanojets powered by biocatalytic reactions. *J. Am. Chem. Soc.* **138**, 13782–13785 (2016).
43. J. R. Howse *et al*., Self-motile colloidal particles: From directed propulsion to random walk. *Phys. Rev. Lett.* **99**, 048102 (2007).
44. M. Ibele, T. E. Mallouk, A. Sen, Schooling behavior of light-powered autonomous micromotors in water. *Angew. Chem.* **48**, 3308–3312 (2009).
45. M. Tătulea-Codrean, E. Lauga, Artificial chemotaxis of phoretic swimmers: Instantaneous and long-time behaviour. *J. Fluid Mech.* **856**, 921–957 (2018).
46. A. Libchaber, From biology to physics and back: The problem of Brownian movement. *Annu. Rev. Condens. Matter Phys.* **10**, 275–293 (2019).
47. P. Illien *et al*., Exothermicity is not a necessary condition for enhanced diffusion of enzymes. *Nano Lett.* **17**, 4415–4420 (2017).
48. D. L. Nelson, M. M. Cox, *Lehninger Principles of Biochemistry* (Macmillan, 2017).
49. R.-L. Zheng, R. G. Kemp, Phosphofructo-1-kinase: Role of charge neutralization in the active site. *Biochem. Biophys. Res. Commun.* **214**, 765–770 (1995).
50. C. K. Mathews, K. E. van Holde, K. Ahern, "Metabolism of nitrogenous compounds: amino acids, porphyrins, and neurotransmitters" in *Biochemistry* (Addison Wesley Longman, ed. 3, 1999), pp. 743–793.
51. D. Susan-Resiga, T. Nowak, Proton donor in yeast pyruvate kinase: Chemical and kinetic properties of the active site Thr 298 to Cys mutant. *Biochemistry* **43**, 15230–15245 (2004).
52. K. K. Tsuboi, K. Fukunaga, C. H. Chervenka, Phosphoglucose isomerase from human erythrocyte preparation and properties. *J. Biol. Chem.* **246**, 7586–7594 (1971).
53. B. Krajewska, I. Ureases, Functional, catalytic and kinetic properties: A review. *J. Mol. Catal. B Enzym.* **59**, 9–21 (2009).
54. B. Krajewska, M. Brindell, Thermodynamic study of competitive inhibitors' binding to urease. *J. Therm. Anal. Calorim.* **123**, 2427–2439 (2016).
55. P. Tougard *et al*., Structural and functional properties of mutant Arg203Pro from yeast phosphoglycerate kinase, as a model of phosphoglycerate kinase-Uppsala. *PEDS* **9**, 181–187 (1996).
56. O. Ijeoma, H. N. Hollowell, M. A. Bodnar, B. M. Britt, Thermodynamic analysis of the nondenaturational conformational change of baker's yeast phosphoglycerate kinase at 24° C. *Arch. Biochem. Biophys.* **478**, 206–211 (2008).
57. P. Govindjee, *V2: Development, Carbon Metabolism, and Plant Productivity* (Elsevier, 2012).
58. Y. S. Kulkarni *et al*., Enzyme architecture: Modeling the operation of a hydrophobic clamp in catalysis by triosephosphate isomerase. *J. Am. Chem. Soc.* **139**, 10514–10525 (2017).
59. R. Dave, D. S. Terry, J. B. Munro, S. C. Blanchard, Mitigating unwanted photophysical processes for improved single-molecule fluorescence imaging. *Biophys. J.* **96**, 2371–2381 (2009).
60. Q. Zheng *et al*., Ultra-stable organic fluorophores for single-molecule research. *Chem. Soc. Rev.* **43**, 1044–1056 (2014).